2

Refraction surveying

J.-L. Mari

Seismic refraction was the first technique used in oil exploration. During the 1920-1960s, the refraction method allowed the detection of salt domes in the United States, the mapping of large extend structures in Iran, and oil field discoveries in the Algerian Sahara. However, from the 1930s seismic reflection became the predominant seismic method and the refraction method was used for the computation of static corrections.

Today, the refraction method provides a quick reconnaissance-mapping tool for delineating near-surface velocity structures and/or their associated static corrections. It requires only the measurement of the arrival times of first arrival waves (direct and refracted waves) to provide a geological model, whereas the reflection method requires a complete processing of the recorded wavefield. The picking of first arrivals is much easier than the identification and picking of other events.

DOI: 10.1051/978-2-7598-2351-2.c004

Seismic refraction is currently used in civil engineering and hydrogeology for targeted depths of less than 300 m (Mari *et al.*, 1999). The method is particularly suited for the following studies:

In civil engineering:

- Preliminary studies for construction sites,
- Determination of the near surface structures,
- Rock mechanics (rippability, Poisson's ratio),
- Search for cavities.

In hydrogeology:

- Highlighting channels carved in bedrock,
- Highlighting fractured areas in bedrock,
- Measurement of water table depth.

2.1 Refraction surveying: Plus-Minus and GRM methods

Refraction-based velocity estimation of the subsurface is conventionally carried out using well-known methods, such as the Hagedoorn's Plus-Minus method (1959) or the generalized reciprocal method (GRM) proposed by Palmer (1986), which provides simple models of the subsurface defined by refractors with simple geometry and a relatively constant velocity distribution. The GRM method is widely used in refraction prospecting (Ge *et al.*, 2010). It assumes that first arrivals only originate from critical refraction and lateral continuous refractors with relatively simple velocity distributions. The method becomes less accurate as subsurface variability increases. It is used for shallow investigations and to determine weathering corrections in refraction and reflection surveys.

Refraction imaging of the subsurface is based on the analysis of refraction time-distance curves. The arrival time t(x) of the refracted wave is given by the following relationship:

$$t(x) = x.\cos(\varphi)/ VR + \delta(0) + \delta(x) \quad (2.1)$$

- x: source – receiver distance
- φ: dip of refractor over spread length
- VR: refractor velocity
- δ(0): delay time at source point
- δ(x): delay time at receiver point

Equation (2.1) can be rewritten as follows:

$$t(x) - x.\cos(\varphi)/ VR = \delta(0) + \delta(x) \quad (2.2)$$

Equation (2.2) is called the T – X/V curve.

To obtain the true velocity of each marker, its dip and thickness, time-distance curves in both directions are required, i.e. up-dip shooting and down-dip shooting (direct and reverse shots), as shown in Figure 2.1. This requires recordings where geophones are aligned with shot points. Such an implementation makes it possible to measure two apparent velocities Va1 and Va2 and two intercept times I1 and I2 on time-distance curves associated with the refractor.

For shot 1 (up-dip), the following relationships apply:

$$t(x) = x/Va1 + I1 \text{ with } V1/Va1 = \sin(i_c + \varphi) \text{ and } I1 = 2H1.\cos(i_c)/V1$$

For shot 2 (down-dip), the following relationships apply:

$$t(x) = x/Va2 + I2 \text{ with } V1/Va2 = \sin(i_c - \varphi) \text{ and } I2 = 2H2.\cos(i_c)/V1$$

The measurements of the two apparent velocities Va1 and Va2 of the refraction time-distance curves, and the velocity V1 of the direct wave in the first layer, enable the determination of the critical angle i_c, the refractor velocity VR ($V1/VR = \sin(i_c)$), its dip φ, and the thicknesses (H1 and H2) of the layer at the vertical of the two shot points.

The method, known as the intercept-time method, is illustrated in Figure 2.1 for a single layer over a substratum. It can be extended to multilayer models (Palmer, 1986).

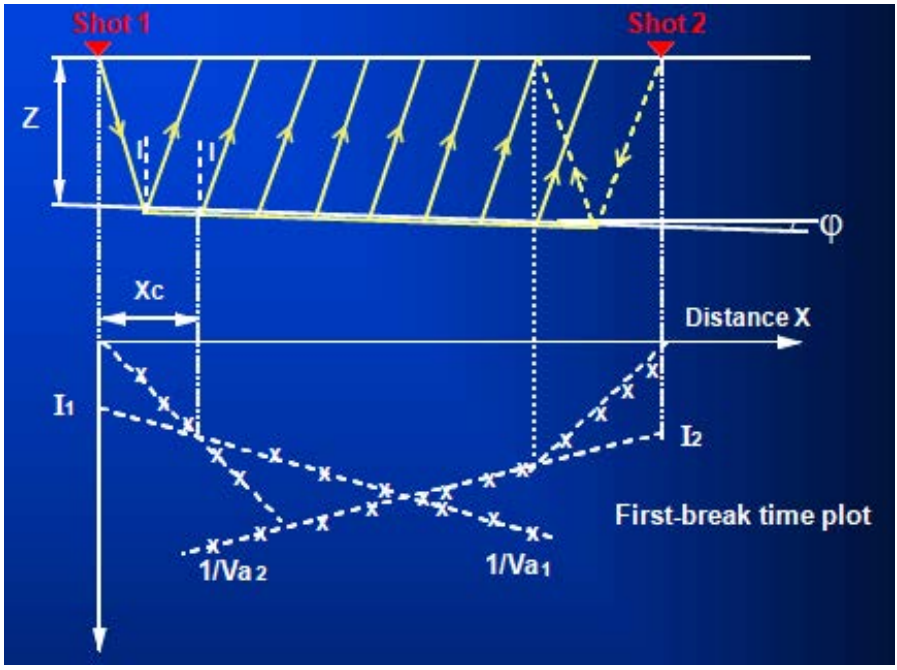

Figure 2.1 *Intercept-time method.*

The direct and reverse shots allow the differentiation between anomalies due to the topography and anomalies associated with the refractors, as shown in Figure 2.2. In the synthetic example, the model is a single layer over a substratum. The waves are refracted by the substratum. The topography is flat with a small rectangular horst. The substratum is flat, with a vertical fault. This Figure shows, from top to bottom:

- Time-distance curves for the arrival times of the waves refracted from the substratum. The red curve corresponds to a direct shot located on the left; the blue curve corresponds to a reverse shot located on the right. It can be seen that the anomaly due to the topography is located on the T-X curves at the same abscissas X.
- The geological model. The raypaths associated with the direct and reverse shots (red and blue lines) are shown within the model.
- T-X/V curves. On the T-X/V curves, the anomalies due to the topography are in phase; the anomalies due to the substratum are shifted laterally in distance. The distance between the anomalies of the 2 curves is the double offset or critical distance (X_c = 2h. tg(i_c)). The two T-X/V curves must be shifted in opposite directions towards their associated shot point to put in phase the anomalies due to the substratum (fault) at the location of the geological feature (fault). The distance of the shift is the single offset (half the critical distance).

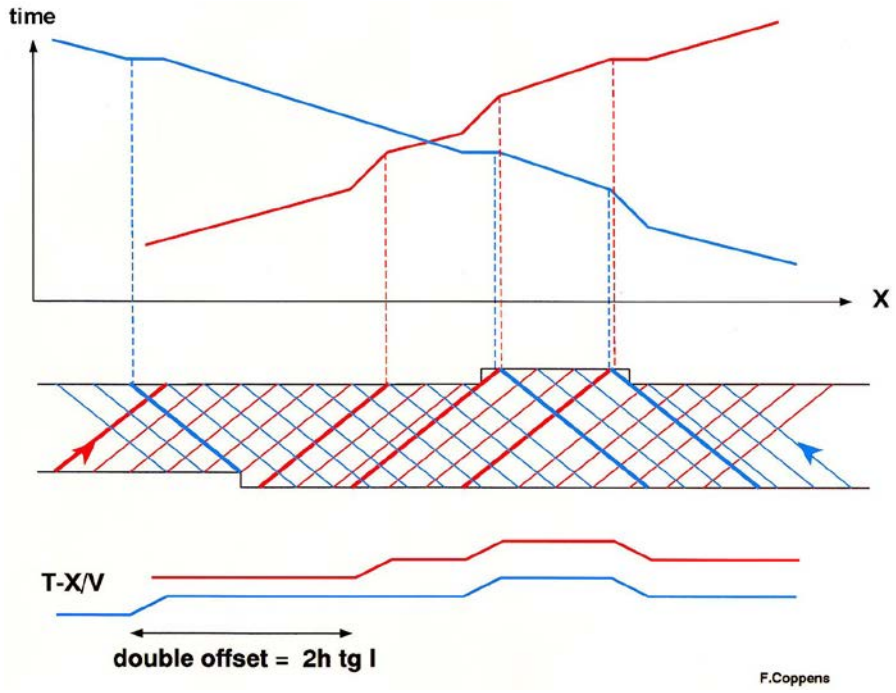

Figure 2.2 *Seismic anomalies on T-X curves.*

Picked times of direct and reverse shot points (Figure 2.3) give access to the t^+ and t^- curves which allow the computation of the refractor velocity analysis function, t_V and the generalized time-depth or delay time, t_G respectively. The analysis of the travel time data proceeds in two stages, with the computation of seismic velocities followed by the depth computations.

Formulae for the computation of the velocity analysis function t_V and time-depths t_G are given in Chapter 8 of "Refraction seismics", (Palmer, 1986). The symbols used are defined in Figure 2.3.

The refractor velocity analysis function, t_V at position G (Figure 2.3-a), is defined by the equation:

$$t_V = \frac{1}{2} t_G^- = \frac{1}{2}\left(t_{AY} - t_{BX} + t_{AB}\right) \tag{2.3}$$

This function is computed for each pair of forward and reverse arrival times, t_{AY} and t_{BX} and the reciprocal time, t_{AB}. The value of the function is referenced to G, which is midway between X and Y, and it is plotted as a function of the distance AG. Equation (2.3) is a linear relation between t_V and the distance AG. Considering a multi-layer model with a plane dipping interface, the slope or gradient of this equation is taken as the inverse of an apparent velocity, V_n', where:

$$\frac{d}{dx} \cdot t_V = 1 / V_n'$$

If dip angles are reasonable, and appear planar over a Fresnel zone, the relation between the true refractor velocity V_n and the apparent velocity, V_n', is:

$$V_n \approx V_n' \cos\theta_{n-1} \text{ with } \theta_{n-1} \text{ the true dip angle of layer } n\text{–}1$$

In general, V_n' is usually taken as the true refractor velocity.

The generalized time-depth, t_G at position G (Figure A1-b), is defined by:

$$t_G = \frac{1}{2} t_G^+ = \frac{1}{2}\left(t_{AY} + t_{BX} - \left(t_{AB} + XY / V_n'\right)\right) \tag{2.4}$$

The relationship between layer thicknesses and the generalized time-depth is:

$$t_G = \sum_{j=1}^{n-1} Z_{jG}\left(\cos\alpha_{jn} + \cos\beta_{jn}\right) / 2V_j \tag{2.5}$$

where α_{jn}, β_{jn} are the ray path angles of incidence at interface j, V_j is the interval velocity of layer j, and Z_{jG} is the thickness of layer j at surface position G.

The depth conversion can be conveniently approximated with the zero-dip expression:

$$t_G = \sum_{j=1}^{n-1} Z_{jG}\left(\cos\phi_{jn}\right) / V_j \text{ with } \sin\left(\phi_{jn}\right) = V_j / V_n \tag{2.6}$$

where ϕ_{jn} are the ray path angles of incidence at interface j if the dip angle θ_j of layer j is 0.

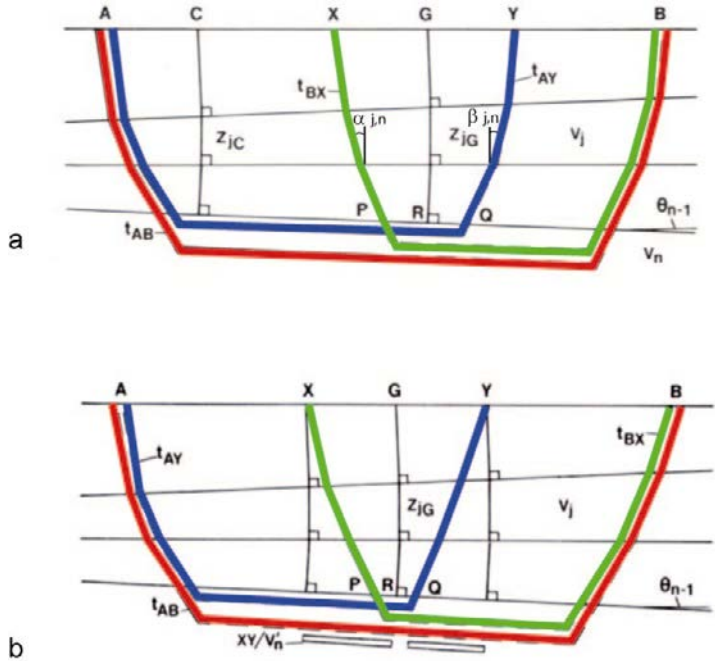

Figure 2.3 *GRM method.*

Figures 2.3-a and b are schematics of the ray paths used in the calculation of both the velocity and the shape of the refractor. For a value of XY such that the forward and reverse rays emerge from nearly the same point on the refractor, i.e. P, R and Q coincide, as shown in Figure 2.3, a result similar to the mean of the migrated forward and reverse delay times is obtained. At the optimum value of XY (P and Q are coincident), accurate velocities can be measured with deep or irregular refractors and the maximum definition of the refractor can be recovered from the travel time data (Palmer, 1986). The Plus-Minus method (a simplified version of the GRM method with XY=0) assumes that first arrivals only originate from critical refraction and laterally continuous refractors with relatively simple velocity distributions.

Figure 2.4 is an example of a refraction survey. The refraction line is rectilinear. In the acquisition of data, a 48-channel recorder was used. An explosive source (25 g) was detonated and a single geophone (10 Hz) per trace was deployed. Such a source makes it easy to identify and pick first arrivals. The distance between two adjacent geophones was 5 m. A direct shot and a reverse shot were recorded (Figure 2.4, top). To obtain the velocity of the refractor (top of the reservoir) and its depth, the Plus-Minus method was used. This method requires geophones to be aligned with shot points. The arrival times of the direct and refracted waves have been picked on the two in-line shots. The picked times from the in-line shots (direct and reverse) have been used to compute the t^- and the t^+ curves to obtain the velocity V2 of the

refractor and the generalized time-depth curve. The t^- curve (Figure 2.4, bottom) can be approximated by a straight line, the slope of which gives the velocity of the refractor, which was found to be 3,350 m/s. The slope of the direct wave gives the velocity V1 of the medium situated above the refractor. The medium situated above the refractor is defined as the weathering zone (Wz). Its velocity was found to be 850 m/s. The generalized time-depth, t_G, also called delay time, shows the shape in time of the refractor (Figure 2.4, bottom).

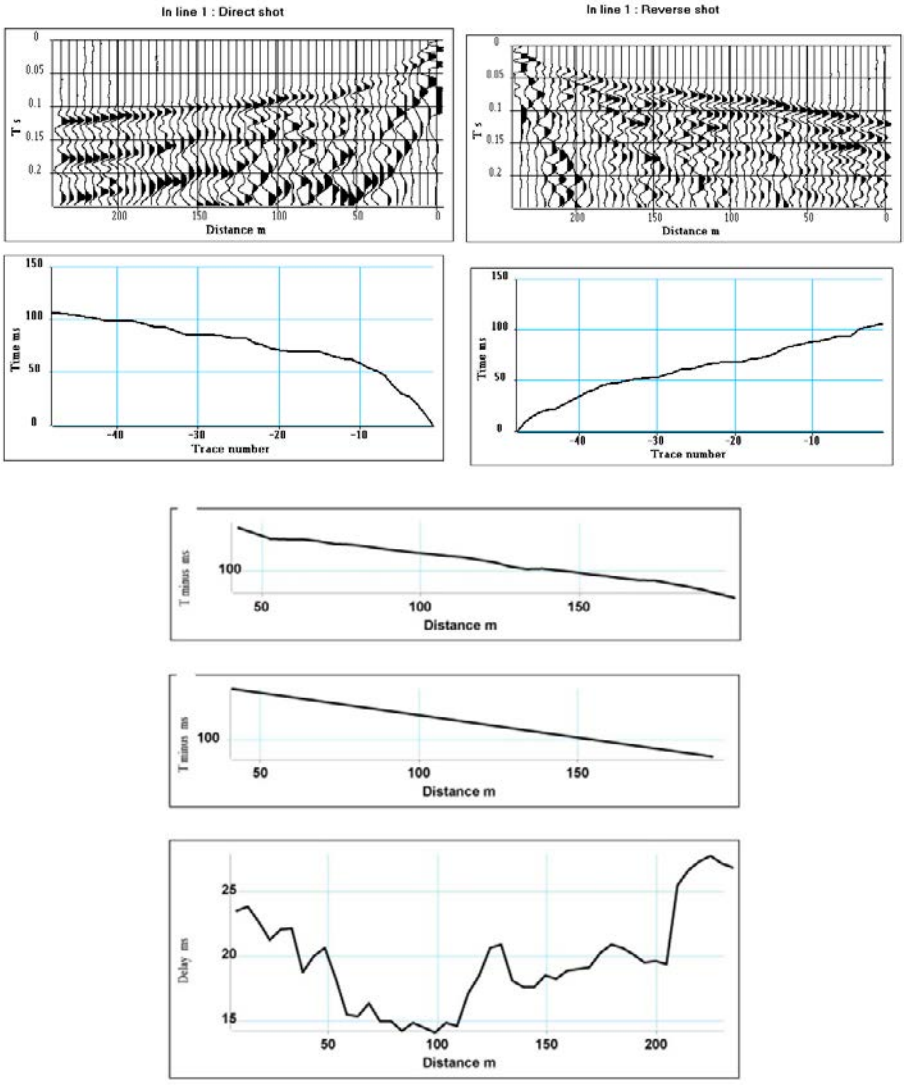

Figure 2.4 *Example of a refraction survey with the Plus-Minus method.*

2.2 Amplitudes of refracted waves

Amplitudes of refracted waves, also called head waves, are not commonly used in seismic refraction studies. Nikrouz (2016) has conducted an interesting synthesis of the relationship between head wave amplitudes and seismic refraction velocities, showing through field studies that variations in amplitudes are associated with velocity changes in the refractor: the higher the contrast in the refractor wave velocity, the lower the head wave amplitude and vice versa (Palmer, 2001). Heelan (1953) and Werth (1967) have shown that the amplitude of a head wave for a thick reflector with a plane horizontal interface is K.G.F(t) where:

- K is the head coefficient which is a function of seismic velocities and densities in the upper layer and the refractor. Werth (1967) expressed K as:

$$K = \frac{2\rho\chi\gamma\left[\lambda_1\left(1+2m\gamma^2\right)+\lambda_2\left(\rho-2m\gamma^2\right)\right]^2}{\left(1-\gamma^2\right)^{1/2}\left[\gamma^2\left(1+2m\gamma^2-\rho\right)+\rho\chi\lambda_2+\chi\lambda_1\left(1+2m\gamma^2\right)^2\right]^2}$$

$$\gamma = V_{P1}/V_{P2}$$

$$\rho = \rho_1/\rho_2$$

$$m = \rho\left(V_{S1}^2/V_{P1}^2\right)-\left(V_{S2}^2/V_{P1}^2\right)$$

$$\chi = \left(1-\gamma^2\right)^{1/2}$$

$$\lambda_1 = \left(V_{P1}^2/V_{S1}^2-\gamma^2\right)^{1/2}$$

$$\lambda_2 = \left(V_{P1}^2/V_{S2}^2-\gamma^2\right)^{1/2}$$

  where V_{P1}, V_{S1} and ρ_1 are, respectively, the P-wave velocity, the S-wave velocity and the density in the upper medium 1; and V_{P1}, V_{S2} and ρ_2 are, respectively, the P-wave velocity, the S-wave velocity and the density in the lower medium 2. The variations of K for a set of elastic parameters can be decreased as the contrast in velocities V_{P2} / V_{P1} is increased (Figure 2.4-a). Figures 4-b to d show variations of K versus V_{S2} / V_{S1} for V_{P2} / V_{P1} ranging from 1.1 to 2, in 3 cases: V_{P1} = 1,700 m/s and V_{S1} = 500 m/s, V_{P1} = 2,000 m/s and V_{S1} = 1,000 m/s, V_{P1} = 2,400 m/s and V_{S1} = 1,600 m/s.
- G is the geometric spreading component given by $1/((rL^3)^{1/2})$ where r is the shot-receiver distance and L is the distance the wave has travelled within the refractor. The geometric spreading component is the major contributor of head wave amplitude.
- F(t) is the displacement potential of the incident pulse.

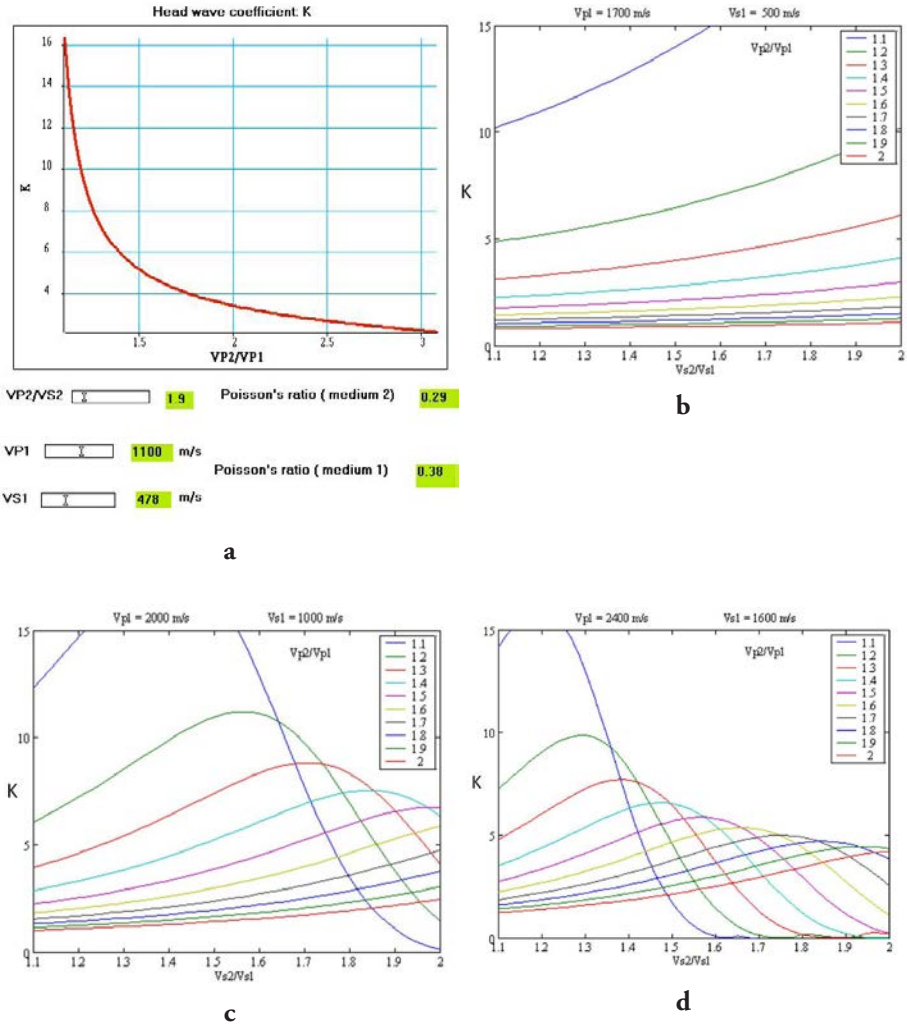

Figure 2.5 *Head wave coefficient.*

The geometric spreading component G must be removed to detect the amplitude variations related to changes in the refractor. In the case of an irregular interface, the refracted wave can be corrupted by converted or diffracted waves, which introduce distortions of the refracted signal. The distortion of the refracted P-wave can be measured by a qualitative dimensionless attribute known as the Shape Index (Ic), which is given by the ratio A2+A3 to A1 where A1, A2 and A3 are the amplitudes of the first three picks of the refraction wavelet. Use of the Shape Index

for acoustic logging was introduced in the 1980s (Lebreton and Morlier, 1983) and then extended to near surface refraction data, as shown in the hydrogeology field case.

2.3 Recommendations for refraction surveying

For refraction surveying, the most favorable conditions are:

- Layer velocity must increase with depth,
- Limited number of markers,
- Weak dips,
- Mostly homogeneous overburden,
- Limited lateral velocity variation.

The choice of implementation parameters (minimum offset, distance between traces, and length of receiver spread) is made by recording refraction shots in the field with a large number of traces covering a wide range of offsets. Analysis of the refraction shot T-X curves enables the definition of the implementation parameters to track a refractor and to predict the modifications of the refraction spread as a function of refractor depth.

The targeted depth defines the minimum offset, it also conditions the receiver spread length. The refraction method is only usable if the refractor velocity (V_R) is clearly discernable from the velocity of the overlying or surrounding layer ($V_R > V_M$). For an accurate measurement of the velocity of the first layer, the distance between the geophones can be reduced (by 1 or 2m) close to the shot point.

To obtain an accurate T-X curve, the refractor must be tracked over a sufficiently large range of offsets. In practice, with a targeted depth h, the total spread length must be 3 to 5 times the depth h. However, if the refractor is a thin bed, the portion of the T-X curve associated with it will not be detected. The seismic refraction method is then “blind”. Another problem that limits the use of refraction seismic surveying is the presence of velocity inversions. For example, for a four-layer model with velocity distributions of: V1<V2>V3<V4, the V3 layer would not appear on the T-X curve. The result of this phenomenon would be an overestimation of depths for the top of layer V4. In the case of lateral velocity variations, the T-X curve can be very complex and difficult to interpret. For the surface detection of a buried structure, the a/h ratio between the size and the depth of the buried structure must be between 2 and 3.

Seismic lines must be laid out in order to facilitate the interpretation of the T-X curves as much as possible. Refraction lines must be rectilinear to avoid errors in the interpretation of the T-X curves. If possible, the receiver spread must be laid out on a plane surface to avoid topographic effects (Figure 2.2).

Refraction seismic surveying is widely used for near surface applications and can be carried out with light field equipment (Figure 2.6):

- A seismic recorder (48 to 96 channels),
- A set of sensors (geophones, hydrophones for marine surveys),
- Cables or streamers,
- Seismic sources (explosive, hammer, weight drop…).

a

b

c

d

e

f

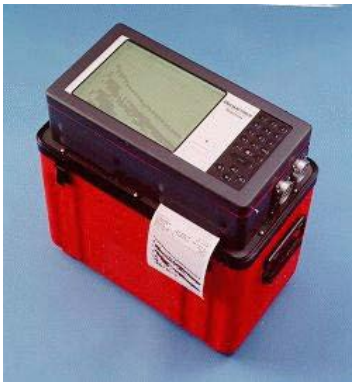

g

h

Figure 2.6 *Field equipment. Source: explosive, gun, weight drop (a, b, c: Apec document); sensors: vertical and horizontal geophones (d, e: IFPEN document), cables (f: IFPEN document); recorders: Geometrics Strataview (g: IFPEN document), Geometrics geode (h: GEO2X document).*

2.4 First example of a seismic refraction application: static corrections

In land seismic acquisition, the elevation differences added to lateral variations in the velocities of the shallow layers cause delays in the arrival times, which vary from trace to trace. Given that these delays are constant with time, the corrections calculated to compensate for them are referred to as "static corrections".

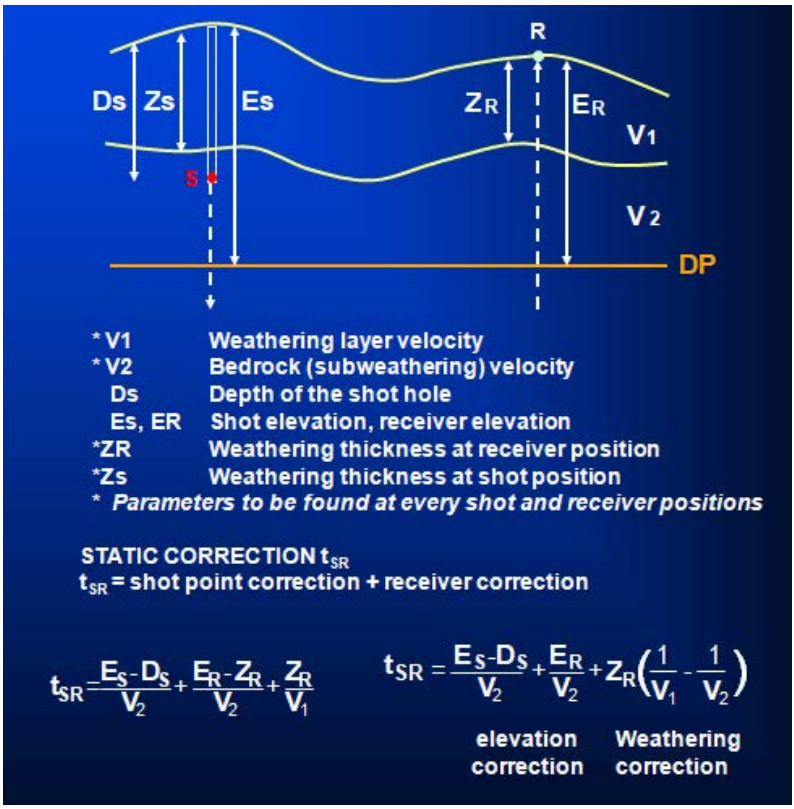

Figure 2.7 *Static corrections. Compensation for delays caused by surface weathering.*

On a seismic record, the event corresponding to a reflection on a seismic horizon no longer forms a hyperbola. The associated t, x (time - distance) curve is distorted due to the surface effects. The surface layer with a variable velocity along the seismic profile is known as the WZ layer, the weathered zone or weathering (Figure 2.7).

The objective of calculating static corrections is to adjust the times of the various traces to simulate the situation where the shots and receivers are on the same surface plane, below which the velocity is constant along the profile. This surface is called the "reference plane" or the "datum plane", abbreviated as DP.

In calculating static corrections, the assumption is that the emergence angle is very small, i.e. the raypaths in the weathered zone (and in practice above the DP) are vertical. The static correction for a given trace is then only a function of the geographical position of the source and receiver and is independent of the source-receiver offset. In some cases this assumption may not be correct: if the emergence angles are not very small, then offset-dependent static corrections must be applied.

Various data are used for the computation of static corrections depending on the location of the line and the land acquisition technique, such as:

- Up-hole or down-hole surveys (Mari and Vergniault, 2018) to obtain the velocity distribution versus depth (Figure 2.8). An up-hole survey gives the absolute static correction at the borehole location. The borehole must be deep enough to reach below the weathering layer. The distance between up-hole surveys on a profile should be less than the spread length to correctly determine long wavelength statics. In practice, close up-hole surveys (more than 2 up-hole surveys per spread length) are needed to make correct correlations between borehole locations. This method, despite the expense due to the need to drill holes, is the best method to use if all the recommendations are followed.
- Weathering shots which are special recordings using a refraction spread designed to determine the thickness and velocity of the weathering layer (Figures 2.1 and 2.4).
- Seismic reflection records. Depending on the geometry designed for the acquisition, the picking of first arrival times (direct and refracted arrivals) provide velocity and delay values (Figure 2.10). If the sources are buried charges, the vertical time VT, also called up-hole time, provides the travel time from the bottom of the borehole.

The total static correction applied to a trace is the sum of the static correction at the source position and the static correction at the receiver position. Determination of the static correction time t_{SR} requires that the elevation, weathered thickness, plus velocities in and below the weathering are known at every point, as illustrated in Figure 2.7.

Below we briefly present the Chronos method, developed by F. Coppens (1985), which provides a set of basic static corrections using constant offset sections and automatic picking. For more details on the Chronos method, the reader should refer to the article by Coppens published in Geophysical prospecting (1985).

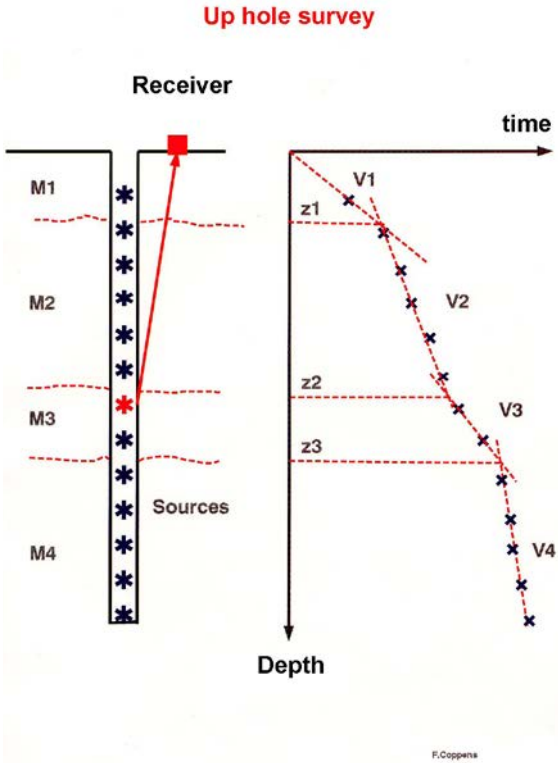

Figure 2.8 *Up-hole survey.*

The calculation of static corrections is based on the measurement of first arrival times. The geophysicist's task is made easier with the use of automatic picking algorithms (Hatherly, 1982; Gelchinsky and Shtivelman, 1983; Coppens, 1985).

Figure 2.9-a shows a seismic record and the 255 m constant offset section, the arrow on the shot point indicating the selected trace. The seismic source is a weight drop. On the constant offset section, the refracted signal evolves very little from trace to trace, which helps with the identification of first arrivals.

The Chronos method is based on the criterion of a sudden energy increase associated with the arrival of a refracted wave. Each seismic trace is transformed into an energy trace representing the ratio between the energy contained in a small sliding window W_2, and the cumulative energy contained in a window W_1, which starts at time zero and ends at the end of window W_2 (Figure 2.9-b). The abscissa τ_0 of the maximum of the energy function gives the approximate time of the refracted arrival. The exact time is then accurately determined by picking the extreme (peak or trough) closest to τ_0 (Figure 2.9-b). If it is an impulsive source, the measured time is reduced by the rise time.

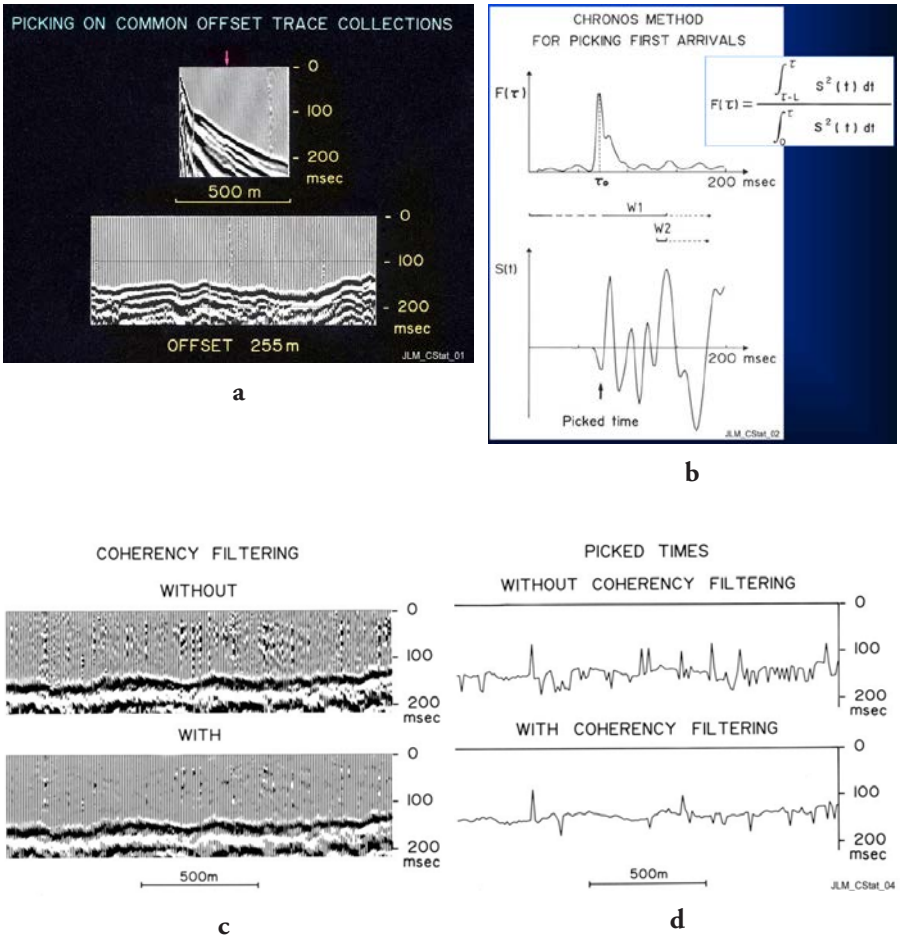

Figure 2.9 *Automatic process for first arrival picking (Coppens, 1985).*

To improve the picking in noisy traces, it is recommended that a spatial coherency filter is applied to seismic traces sorted in constant – offset gathers. Figure 2.9-c shows the efficiency of the coherency filtering on a noisy constant – offset section. The associated picked times are shown in Figure 2.9-d. The number of erroneous picks was considerably reduced. The remaining erroneous values can be edited manually or filtered by a median filter (Mari *et al.*, 1999, 2015).

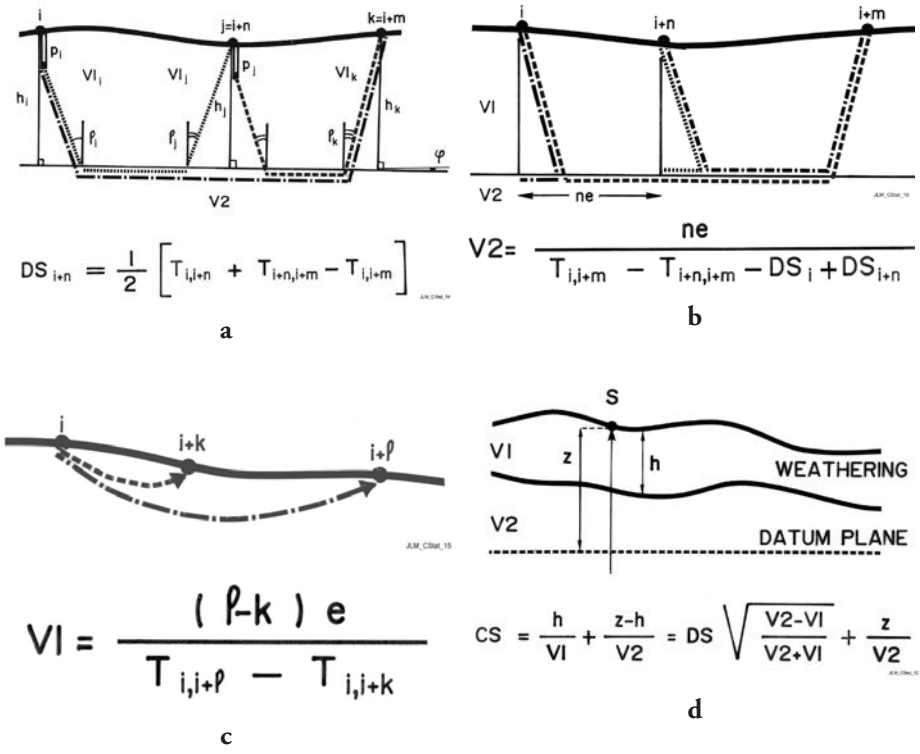

$$DS_{i+n} = \frac{1}{2}\left[T_{i,i+n} + T_{i+n,i+m} - T_{i,i+m}\right]$$

$$V2 = \frac{ne}{T_{i,i+m} - T_{i+n,i+m} - DS_i + DS_{i+n}}$$

$$VI = \frac{(\ell - k)\, e}{T_{i,i+\ell} - T_{i,i+k}}$$

$$CS = \frac{h}{VI} + \frac{z-h}{V2} = DS\sqrt{\frac{V2-VI}{V2+VI}} + \frac{z}{V2}$$

Figure 2.10 *Chronos method (Coppens, 1985).*

Coppens showed that picking two traces per shot, i.e. two constant-offset sections on a seismic profile, is sufficient to determine the delay time for each source or receiver location. This method is well adapted to end-on spreads (Figure 2.10). The two constant offsets must be chosen to ensure that the first arrival times on the two selected traces originate from the same refractor as shown in Figure 2.10-a:

- $T_{i,i+n}$ is the arrival time of the refracted wave with the source located at position i and the receiver at position j= i + n, the source receiver distance being n (near offset).
- $T_{i,i+m}$ is the arrival time of the refracted wave with the source located at position i and the receiver at position i + m, the source receiver distance being m (far offset).
- $T_{i+n,i+m}$ is the arrival time of the refracted wave with the source located at position i + n and the receiver at position i + m, the source receiver distance being m -n (near offset). Consequently, the far offset (m=2n) is the double of the near offset (n).
- The arrival times $T_{i,i+n}$, $T_{i,i+m}$ and $T_{i+n,i+m}$ are used to calculate the delay DS_{i+n} at position j= i + n.

Determining the delay times, and the arrival times of the refracted wave picked on the two constant-offset sections, enables the calculation of the refractor velocity at any point (Figure 2.10-b).

Picking the direct arrival on geophones close to the shot point provides the weathered zone velocity (Figure 2.10-c). Determining the delay, the refractor velocity and the velocity of the weathered layer enables the calculation of the static correction at any point (Figure 2.10-d).

Figure 2.11 and 2.12 are an example of the results obtained using the Chronos method. Figure 2.11 shows, from top to bottom, the variation of velocity V1 of the weathered zone along the line, the variation of the refractor velocity, the delay time curve, the topography and the static correction curve. The static correction curve shows an anomaly between shot points 60 and 110. Figure 2.12 shows the seismic section processed with the static corrections presented in Figure 2.11.

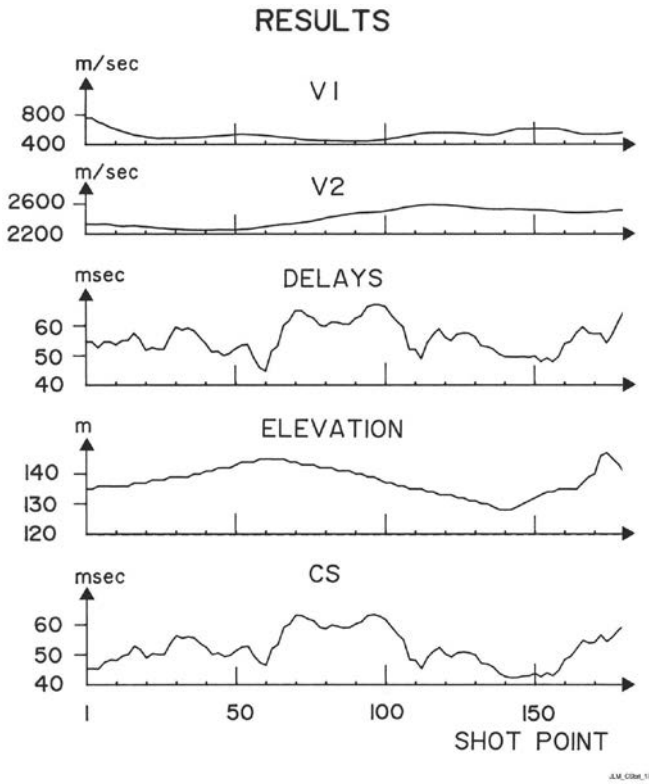

Figure 2.11 *Static corrections with the Chronos method (Coppens, 1985).*

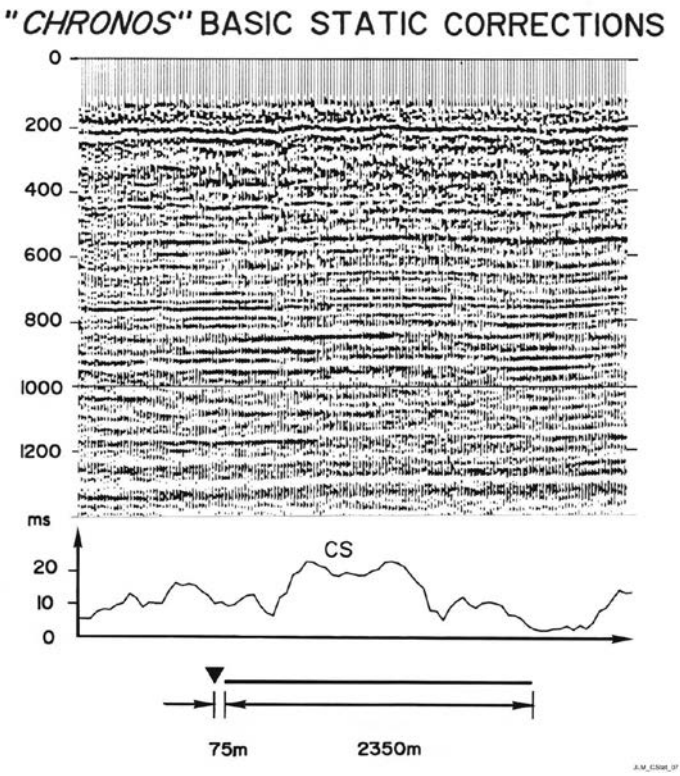

Figure 2.12 *Seismic section processed with static corrections computed by the Chronos method (Coppens, 1985).*

2.5 Second example of a seismic refraction application: Hydrogeology

The University of Poitiers (France) has a Hydrogeological Experimental Site (HES) built near the campus for the sole purpose of providing facilities to develop long-term monitoring and experiments for a better understanding of fluid flow and transfers in fractured rocks (Bernard *et al.*, 2006; Kaczmaryk and Delay 2007; Bourbiaux *et al.*, 2007). The aquifer concerned, 20 to 130 m in depth, consists of tight karstic carbonates of Middle Jurassic age, and lies on the borderline, named the "Poitou threshold", between the Paris and the Aquitaine sedimentary basins (Figure 2.13-a), covering an area of 12 hectares. The top of the reservoir was initially flat and horizontal, 150 million years ago, but has been eroded and weathered since,

during the Cretaceous and Tertiary ages. It is shaped today as hollows and bumps with a relief reaching up to 35 m. Refraction seismic surveying, described in detail by Mari and Porel (2007), has been used to map the irregular shape of the top of the karstic reservoir.

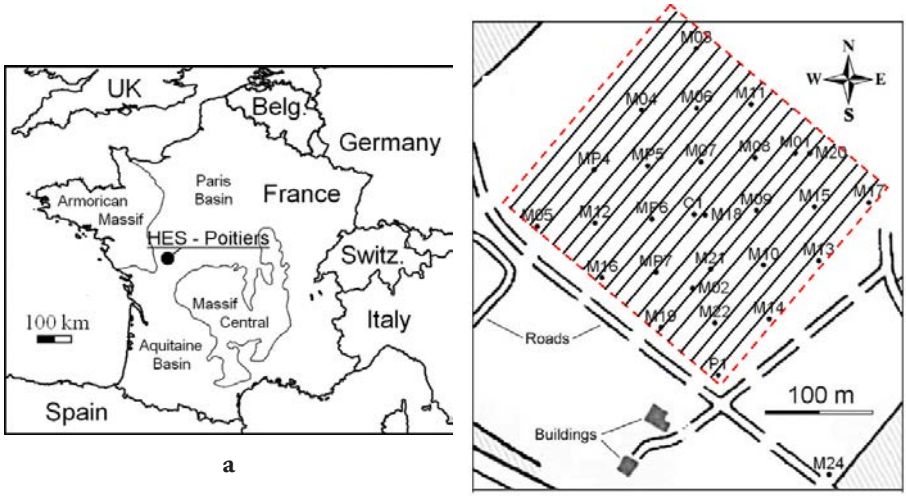

Figure 2.13 *Hydrogeological experimental site in Poitiers. a) location map; b) seismic line implementation.*

Due to the limitations of the area, the length of the seismic line could not exceed 250 m in the in-line direction. In the cross-line direction, the extension of the area does not exceed 300 m. As a result, 20 receiver lines have been implemented, with a 15 m distance between adjacent lines. Figure 2.13-b shows the map locating the seismic lines. A 48-channel recorder was used for the data acquisition. An explosive source (25 g) was detonated and a single geophone (10 Hz) per trace was deployed. The use of this type of source makes it easy to identify and pick first arrivals. A 5 m distance between two adjacent geophones was selected to avoid spatial aliasing.

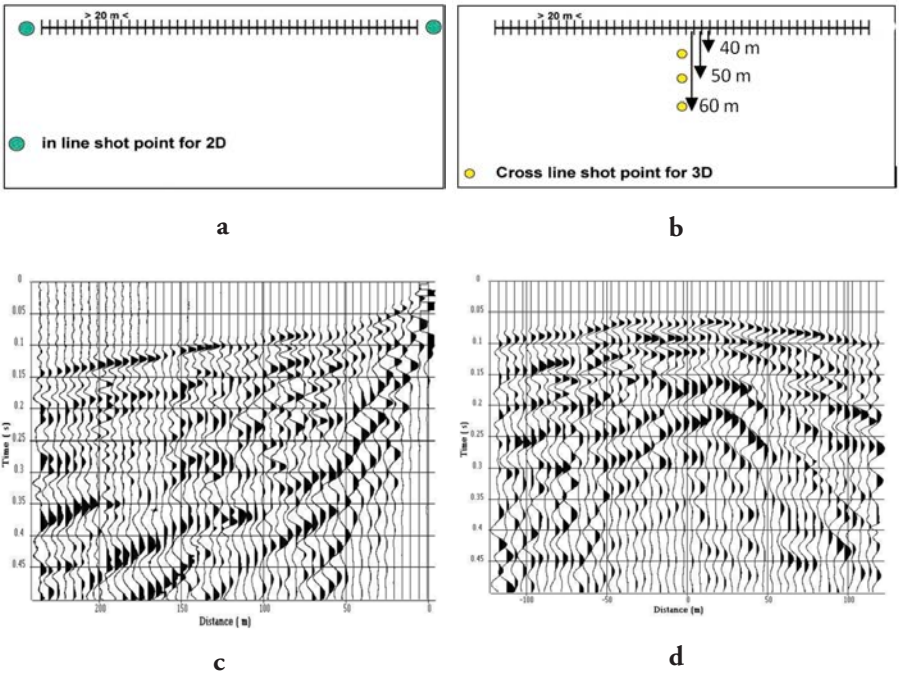

Figure 2.14 *Seismic acquisition. a) 2D in line acquisition geometry, b) 3D cross-line acquisition geometry, c) Example of in-line shot gather, d) Example of cross-line shot gather with 60 m of lateral offset.*

A direct and a reverse shot were recorded per receiver line (Figure 2.14-a). Three shot points in the cross-line direction were fired at distances of 40, 50 and 60 m from the receiver line under consideration (Figure 2.14-b). Figure 2.14-c shows an example of an in-line shot gather and Figure 2.14-d a cross-line shot gather with a lateral offset of 60 m. The range of offsets was selected to optimize the quality of the seismic image over the reservoir depth interval, between 40 and 130 m. The minimum offset distance was chosen as 40 m to reduce the influence of surface waves. The time sampling interval was 0.25 ms and the recording length was 0.5 s.

To obtain the velocity of the refractor (top of the reservoir) and its depth, the Plus–Minus method was used. To apply this method the recordings must be carried out where geophones are aligned with shot points. The arrival times of the direct and refracted waves were picked on all the in-line shots. The picked times from the in-line shots (direct and reverse) were used to compute the t^- and the t^+ curves to obtain the velocity V2 of the refractor and the delay time curve. Figure 2.4 shows the results obtained on line 9. It shows the direct and reverse shot points, the raw t^- curve

and its associated straight-line curve, and the delay time curve. The procedure was applied on each line independently. To obtain a map with a homogeneous sampling interval in both cross-line and in-line directions, the delay time curves were interpolated by kriging with an omni-directional variogram model composed of a nugget effect, a cubic structure with a range of 55 m and a long-scale spherical structure with a range of 145 m (Bourges *et al.*, 2012). Finally, a kriging with the model described above, and a filtering of the nugget effect (random acquisition noise) were performed to obtain the filtered delay time map on a grid 2.5 m x 5m (Figure 2.15-a).

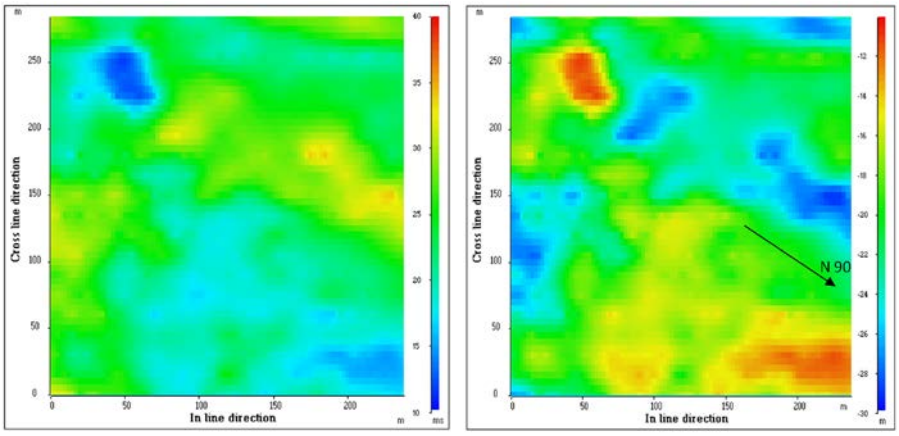

Figure 2.15 *Plus – minus method. a) Delay time map, b) Wz depth map.*

To perform the depth conversion, the velocity of the medium situated above the refractor must be known. Here, it is given by the slope of the direct wave. The medium situated above the refractor is defined as the weathering zone (Wz). In the area, the velocity V_2 of the refractor was found to be 3,350 m/s (from interpretation of the t^- curves), and the velocity of the Wz to be 850 m/s. On the Wz depth map (Figure 2.15-b), the arrow indicates the direction N 90° which corresponds to the main orientation of fracture corridors.

The picked times of the first seismic arrivals on all shots (in-line and cross-line shots), the Wz depth map and the velocity model obtained by the Plus–Minus method are input data for the inversion procedure, called tomography, which can be used to obtain the velocity distribution in depth (Mari and Mendes, 2012). More information on tomography is provided in the following chapter, and readers should also refer to the article by Mari and Mendes published in Near Surface Geophysics (2012).

Figure 2.16 shows the velocity distribution at different depths (15 and 20 m), the 2,500 m/s iso-velocity depth map, and a 3D block with vertical velocity sections located at distances of 0 m, 60 m and 180 m in the cross-line direction and a velocity map located at 20 m in depth. A strong correlation can be seen between the 2,500 m/s iso-velocity depth map (Figure 2.16-c) and the Wz depth map (Figure 2.15-b). The correlation coefficient reaches 0.96.

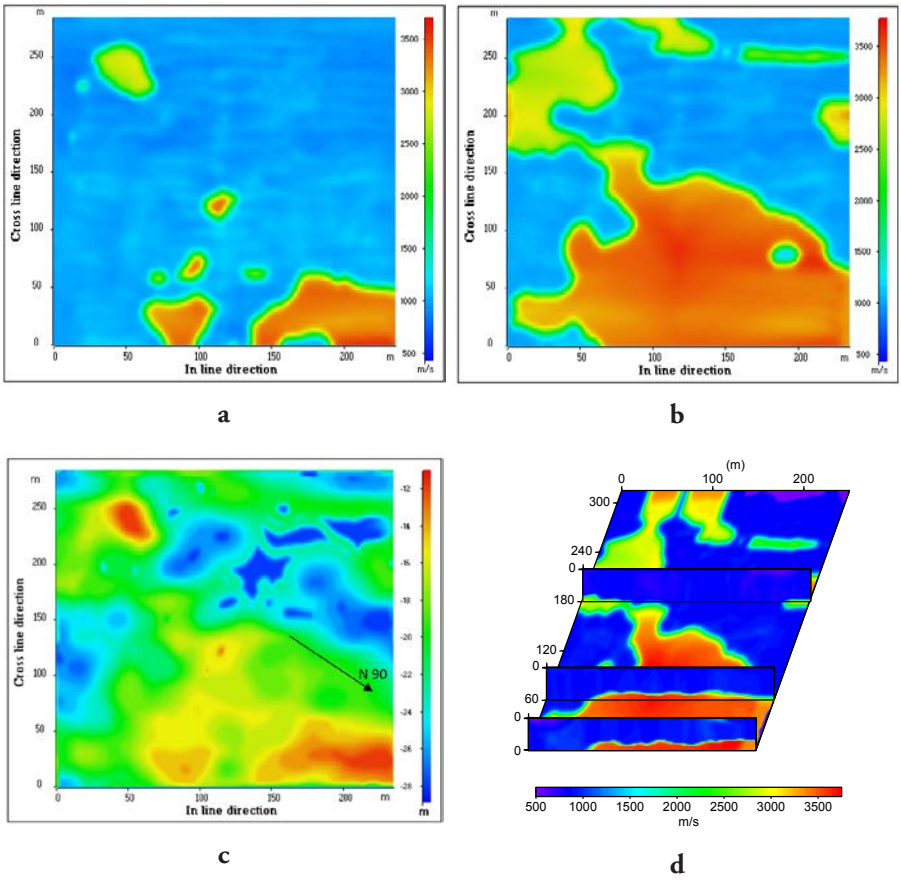

Figure 2.16 *Results of 3D tomography. a) Velocity distribution at 15 m in depth, b) Velocity distribution at 20 m in depth, c) 2,500 m/s iso velocity depth map, d) 3D block with vertical velocity sections located at distances of 0 m, 60 m and 180 m in the cross-line direction and a velocity map located at 20 m in depth.*

The results obtained by the Plus-Minus tomographic inversion joint method can also be used effectively to compute the static corrections in 3D. For that purpose, the thickness H of the weathering zone is given by the 2,500 m/s iso-velocity depth

map. The average velocity V1 in the weathering zone is computed from the velocity distribution obtained by the inversion procedure in the 0-H depth interval. The V2 velocity of the refractor is computed from the velocity distribution obtained by inversion in a narrow depth bandwidth (3 m) situated below the interface located at the depth H. The application to the 3D data is shown in Figure 2.17.

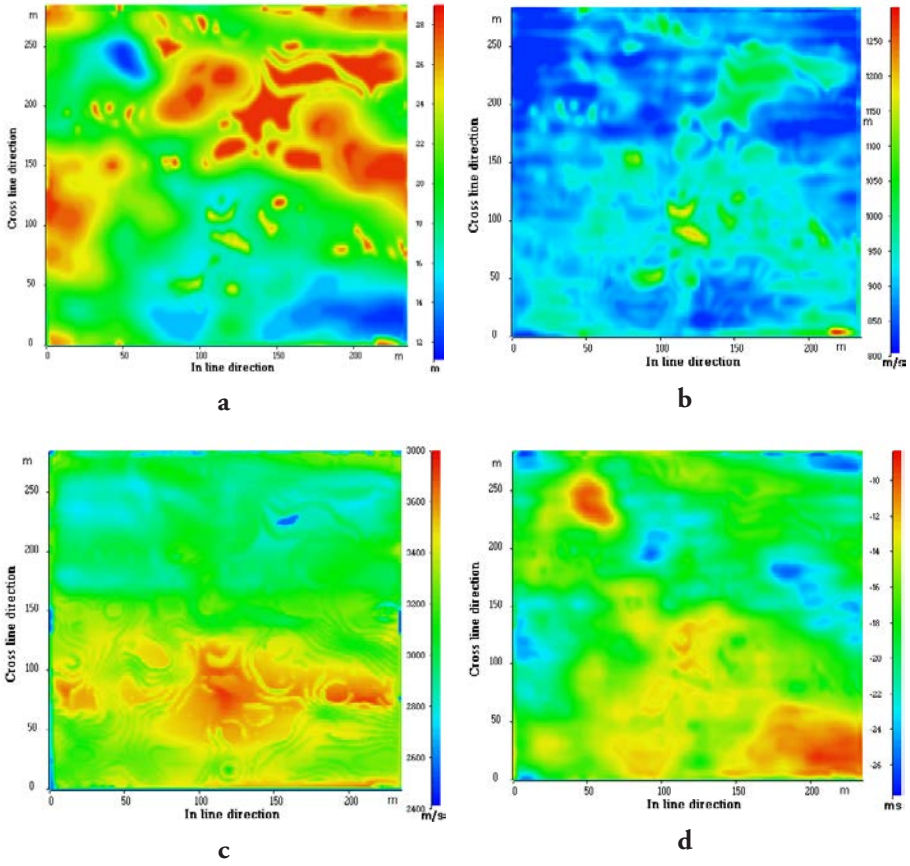

Figure 2.17 *3D static corrections from 3D tomographic inversion. (a) Thickness H of the weathering zone. (b) Average velocity V1 in the weathering zone. (c) Velocity V2 below the weathering zone. (d) 3D static correction map (-H/V1 + H/V2).*

The picked times of the refracted waves were able to provide both a map of the reservoir top (using the T plus –T minus method) and a map of the shape index. Figure 2.18 shows an example of a shot point oriented in the in-line direction before and after the filtering of direct and surface waves. After filtering, a refracted wave is clearly visible, along with interference from refracted – reflected events.

These events are due to heterogeneities and fractures in the bedrock. The shape index map highlights the geological features with an N90 orientation associated with a corridor of fractures (Mari *et al.*, 2018).

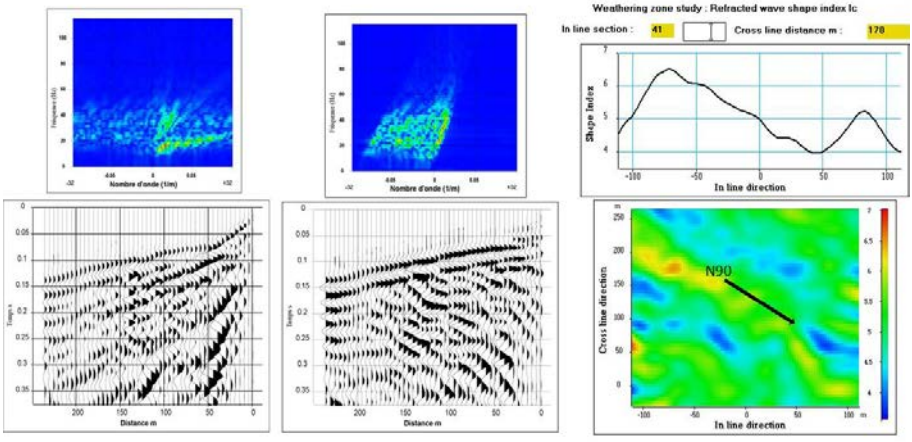

Figure 2.18 *refraction survey: shots before and after the filtering of direct and surface waves, and a shape index map.*

The proposed inversion procedure applied to the field data enables:

- a complete velocity model of the first 35m to be obtained;
- the top of the karstic reservoir to be mapped;
- the detection of the main corridor of fractures, highlighted by a shape index map;
- the calculation of static corrections.

2.6 Conclusion

Seismic refraction can be used for investigations at all depths, but for various technical reasons it is mostly used to study the first 300 meters of the subsurface (spread length, importance of source energy…).

Refracted P-waves are currently used to obtain a velocity model of the near surface by combining conventional methods such as the T plus – T minus method, the GRM method, and tomography. The refraction method is currently used in hydrogeology and civil engineering.

We presented two applications of the refraction method:

- the computation of static corrections,
- the characterization of a near surface karstic reservoir.

For conventional studies, the refraction method only requires the measurement of arrival times of the first arrival waves (direct and refracted waves) to provide a geological model. Amplitudes are not commonly used in seismic refraction studies. A detailed analysis of head wave amplitudes did not generate useful results, however, the fact that head wave amplitude is a function of densities and of seismic velocities suggests that the joint inversion of seismic refraction travel times and head wave amplitudes should facilitate the determination of both seismic velocity and density models (Nikrouz, 2016). Where irregular interface occurs, the analysis of the distortion of the head wave arrival allows the detection of wave interferences, which can be associated with the presence of fractures (second field example).

Seismic refraction is widely used for the study of near-surface layers. Its advantages are:

- only simple equipment required,
- good determination of velocities,
- rapid depth determination.

Unfortunately, it also presents several drawbacks:

- Layer velocity must increase with depth; which is not always the case when dealing with compacted formations;
- A particularly thin layer may completely evade detection; which is even more possible if the velocity contrast is insufficient. In such cases, the determined depths would be incorrect;
- The method is unable to provide highly detailed mapping of structures.

References

Bernard S., Delay F., Porel G., 2006, A new method of data inversion for the identification of fractal characteristics and homogenization scale from hydraulic pumping tests in fractured aquifers, *Journal of Hydrology*, 328, 647-658.

Bourbiaux B., Callot J.P., Doligez B., Fleury M., Gaumet F., Guiton M., Lenormand R., Mari J.L., Pourpak H., 2007, Multi-Scale Characterization of a Heterogeneous Aquifer Through the Integration of Geological, Geophysical and Flow Data: A Case Study, *Oil and Gas Science and Technology, Rev IFP*, 62, 347-373.

Bourges M., Mari J.L., Jeannee N., 2012, A practical review of geostatistical processing applied to geophysical data: methods and applications, *Geophysical prospecting*, 60, 400-412.

Coppens F., 1985, First arrival picking on common offset trace collection for automatic estimation of static corrections, *Geophysical Prospecting*, 33, 1212-1231.

Ge J., Magnani M., Waldron B., 2010, Imaging a shallow aquitard with seismic reflection data in Memphis, Tennessee, USA, Part I: source comparison walk-away tests and the plus-minus method, *Near Surface Geophysics*, 8, 331-340.

Gelchinsky B., Shtivelman V., 1983, Automatic picking of first arrivals and parameterization of travel time curves, *Geophysical Prospecting*, 31, 915-928.

Hagedoorn G.J., 1959, The Plus–Minus method of interpreting seismic refraction sections, *Geophysical Prospecting* 7, 158- 182.

Hatherly P.J., 1982, A computer method for determining seismic first arrival times, *Geophysics*, 47, 1431-1436.

Heelan P.A., 1953, On the theory of head waves, *Geophysics*, 18, 871-893.

Kaczmaryk A., Delay F., 2007, Interference pumping tests in a fractured limestone (Poitiers - France): Inversion of data by means of dual-medium approaches, *Journal of Hydrology* 337, 133-146.

Lebreton F., Morlier P., 1983, Une diagraphie de perméabilité par méthode acoustique, *Bulletin of the International Association of Engineering geology*, n° 26-27.

Mari J.L., Arens G., Chapellier D., Gaudiani P., 1999, *Geophysics of reservoir and civil engineering*, Éditions Technip, Paris, ISBN 2-7108-0757-2.

Mari J.L., Glangeaud F., Coppens F., 1999, *Signal processing for geologists and geophysicists*, Editions Technip, Paris, ISBN 2-7108-0752-1.

Mari J.L., Porel G., 2007, 3D seismic imaging of a near-surface heterogeneous aquifer: a case study, *Oil and Gas Science and Technology, Rev IFP* 63, 179-201, Published online: DOI: 10.2516/ogst/2007077.

Mari J.L., 2015, *Signal processing for geologists & geophysicists*, e-book, DOI: 10.2516/ifpen/2011002, http://books.ifpenergiesnouvelles.fr/ebooks/signal-processing/

Mari J.L. and Vergniault C., 2018, Well seismic surveying and acoustic logging, EDP-Sciences, Les Ulis, DOI: 10.1051/978-2-7598-2263-8, ISBN (eBook): 978-2-7598-2263-8, https://www.edp-open.org/well-seismic-surveying-and-acoustic-logging

Mari J.L., Mendes M., 2012, High resolution 3D near surface imaging of fracture corridors and cavities by combining Plus-Minus method and refraction tomography, *Near Surface Geophysics*, 10, DOI: 10.3997/1873-0604.2011052.

Mari J.L., Lopez A.I, Benjuma B., Garcia-Lobon J.L., 2018, Shape index: a refraction attribute to detect fractures and permeable bodies, paper Th J 12, 80th EAGE annual conference, Copenhagen, Denmark.

Mendes M., 2009, A hybrid fast algorithm for first arrivals tomography, *Geophysical Prospecting*, 57, 803-809. DOI: 10.1111/j.1365-2478.2008.00755.x

Nikrouz R., 2016, Relationship between head wave amplitudes and seismic refraction velocities to detect lateral variation in the refractor, *Journal of the Earth and Space Physics*, 4, 69-76.

Palmer D., 1986, Refraction seismics, *Geophysical Press*, 13.

Palmer D., 2001, Resolving refractor ambiguities with amplitudes, *Geophysics*, 66, 1590-1593.

Palmer D., 2008, Is it time to re-engineer geotechnical seismic refraction methods? *First Break* 26, 69-77.

Werth G.A., 1967, *Method for calculating the amplitude of the refraction arrival*, in: Musgrave A.W. (Ed), seismic refraction prospecting, Society of Exploration Geophysics, 119-137.